



Article

V₃S₄ Nanosheets Anchored on N, S Co-Doped Graphene with Pseudocapacitive Effect for Fast and Durable Lithium Storage

Naiteng Wu ^{1,2,*} , Di Miao ¹, Xinliang Zhou ¹, Lilei Zhang ¹, Guilong Liu ¹, Donglei Guo ¹ and Xianming Liu ^{1,*}

¹ Key Laboratory of Function-oriented Porous Materials, College of Chemistry and Chemical Engineering, Luoyang Normal University, Luoyang 471934, China; miao990831@163.com (D.M.); chevasz@163.com (X.Z.); zhanglilei@outlook.com (L.Z.); glliu@tju.edu.cn (G.L.); gdl0594@163.com (D.G.)

² College of Materials and Chemical Engineering, China Three Gorges University, Yichang 443002, China

* Correspondence: wunaiteng@gmail.com (N.W.); myclxm@163.com (X.L.)

Received: 12 October 2019; Accepted: 13 November 2019; Published: 18 November 2019



Abstract: Construction of a suitable hybrid structure has been considered an important approach to address the defects of metal sulfide anode materials. V₃S₄ nanosheets anchored on an N, S co-doped graphene (VS/NSG) aerogel were successfully fabricated by an efficient self-assembled strategy. During the heat treatment process, decomposition, sulfuration and N, S co-doping occurred. This hybrid structure was not only endowed with an enhanced capability to buffer the volume expansion, but also improved electron conductivity as a result of the conductive network that had been constructed. The dominating pseudocapacitive contribution (57.78% at 1 mV s⁻¹) enhanced the electrochemical performance effectively. When serving as anode material for lithium ion batteries, VS/NSG exhibits excellent lithium storage properties, including high rate capacity (480 and 330 mAh g⁻¹ at 5 and 10 A g⁻¹, respectively) and stable cyclic performance (692 mAh g⁻¹ after 400 cycles at 2 A g⁻¹).

Keywords: V₃S₄ nanosheets; pseudocapacitive; N, S co-doped graphene; lithium ion batteries

1. Introduction

Lithium ion batteries (LIBs) are the dominant energy storage device in the field of mobile devices. A high capacity, high rate, long cyclic life, and safety are the critical elements for their large-scale application [1]. Traditional graphite anodes, on the other hand, could not meet the above requirements. Numerous novel candidates, such as transition metal oxide, sulfide, alloy, and silicon, have been explored to replace the commercial graphite anode material.

Among these anode materials, the earth-abundant and high capacity and transition of multiple valence vanadium-based materials are considered as the most promising candidate for the advanced LIBs [2]. V₂O₃ [3,4], VO₂ [5], V₆O₁₃ [6], and other metal vanadium oxide composites [7–10] have been reported in previous works. However, inferior electric conductivity is a common drawback for these vanadium oxides, resulting in insufficient rate performances [2]. For vanadium sulfides, the moderate V–S bond would decrease the electrochemical polarization and benefit the intercalation and deintercalation of Li⁺ or other alkali metal ions, which would further result in improved electrochemical properties [7]. However, bulk metal sulfides usually suffer from large volumetric expansion (resulting in the obvious capacity fading) and sluggish electron transport kinetics (the cause of the inferior rate property) [8,9]. Construction of nanostructures and composites with conductive substrates are considered an efficient route to overcome the drawbacks of bulk vanadium sulfides. For example, flower-like VS₂ nanosheets [10], VS₄ microsphere@PANI [11], VS₄ nanoparticles@CNTs [12], VS₄

nanowire [13], nanosheets, nanoparticles [14] anchored on graphene, V_2S_3 microsphere@C [15], and V_5S_8 -graphite hybrid nanosheet [16,17] anodes delivered the improved Li^+/Na^+ storage performances. According to the above works, VS_4 microsphere@PANI delivered a capacity of 755 mAh g^{-1} at the 50th cycle under a current density of 0.1 A g^{-1} [11], and the VS_4 /graphene composite exhibited a capacity of 954 mAh g^{-1} at the end of 100 cycles under the same current density [18]. The durable lithium storage under high current density would not be obtained. Furthermore, toxic thioacetamide and hydrogen sulfide are always used as sulfide sources in these synthesis processes. The green synthesis route is still a challenge for the application of vanadium sulfides anode materials.

In this work, V_3S_4 nanosheets anchored on N, S co-doped graphene have been fabricated through a facile and green method. NH_4VO_3 and $(NH_2)_2CS$ were used as vanadium and sulfide sources, respectively. V_3S_4 nanosheets shorten the transmission path of both electron and Li ions. Meanwhile, the formed N, S co-doped graphene aerogel not only endow the as-prepared anode with the enhanced capability to buffer the volume expansion but also construct a conductive network to improve electron conductivity. Moreover, the dominating pseudocapacitive contribution (57.78% at 1 mV s^{-1}) is effective for improving the electrochemical performances. When serving as an anode material for LIBs, V_3S_4 nanosheet anchored on N, S-doped graphene exhibits a high rate capacity (480 and 330 mAh g^{-1} at 5 and 10 A g^{-1} , respectively) and stable cyclic performance at high rate (692 mAh g^{-1} after 400 cycles at 2 A g^{-1}).

2. Materials and Methods

2.1. Materials Synthesis

Synthesis of V_3S_4/N , S-rGO (reduced graphene oxides) nanosheets. In a typical synthesis, $2.5 \text{ mmol } NH_4VO_3$ and $1.4 \text{ g } (NH_2)_2CS$ were dissolved in 20 mL formed GO (graphene oxides) aqueous solution (5 mg mL^{-1}) at $60 \text{ }^\circ\text{C}$. Then, the mixed solution was transferred into a 25 mL Teflon-lined stainless-steel autoclave and heated at $180 \text{ }^\circ\text{C}$ for 20 h in an oven. After hydrothermal treatment, the formed hydrogel was freeze-dried and annealed at $600 \text{ }^\circ\text{C}$ for 5 h under Ar atmosphere to obtain the final samples (denoted as VS/NSG).

2.2. Materials Characterization

X-ray diffraction (XRD, Bruker D8 with $Cu \text{ K}\alpha$ radiation, Billerica, MA, USA) analysis was carried out to determine the crystal structure of the samples. The morphology and the structure of the samples were investigated by SEM (SEM, Sigma 500, Zeiss, Oberkochen, Germany) and transmission electron microscopy (TEM, JEOL JEM2100, Tokyo, Japan). X-ray photoelectron spectroscopy (XPS, EscaLab 250Xi, Shanghai, China) was performed to determine the valence state of the products. The graphitic degree of reduced graphene oxide was investigated by Raman spectrometer with an excitation laser beam wavelength of 633 nm (HORIBA Jobin-Yvon, LabRAM Aramis, Kyoto, Japan). To investigate the content of the coating carbon, thermal gravimetric analysis was conducted on a thermal analyzer (SII TG/DTA6300, Tokyo, Japan) in air at a heating rate of $5 \text{ }^\circ\text{C min}^{-1}$.

2.3. Electrochemical Measurements

V_3S_4 nanosheet anchored on N, S-doped graphene was assembled CR2032 half-coin cells to evaluate its electrochemical performance. The assembly processes were similar to our previous works [19,20]. Typically, the mass loading of active material is about $1.2\text{--}1.3 \text{ mg cm}^{-2}$. The charge-discharge processes were operated at the voltage range of $0.005\text{--}3 \text{ V}$ using Neware CT3008 (Neware, Shenzhen, China). Cyclic voltammetry measurements (CV, at the scanning rate from 0.1 to 1.0 mV s^{-1}) and electrochemical impedance spectroscopy (EIS, in the frequency range from $100,000\text{--}0.01 \text{ Hz}$ with an AC amplitude of 5 mV) were conducted on the Parstat 4000+ workstation (Princeton Applied Research).

3. Results

The preparation process is illustrated in Figure 1a. XRD was firstly conducted to investigate the crystal phase of as-prepared sample. As shown in Figure 1b, most of diffraction peaks of as-prepared sample can be indexed as the standard monoclinic V_3S_4 phase (JCPDS no. 65-3745). The low intensity of diffraction peaks would be ascribed to the crystallinity of the nanosheet and graphene substrate. In Figure 1c, there is an obvious interlayer spacing along the c -axis, which is convenient for the storage of lithium ions. The content of graphene substrate was exposed by TG analysis. After the heat treatment process in air atmosphere, VS/NSG would be decomposed and oxidized to V_2O_5 . In this process, the change of weight is about -3% . According to the results of TG analysis (Figure S1), the content of graphene substrate is about 38 wt %. As shown in Figure S2, VS/NSG exhibits two typical D and G bands at around 1360 and 1585 cm^{-1} , corresponding to sp^3 -type disordered carbon and sp^2 -type ordered graphitic carbon [21,22]. The intensity ratio of G and D band ($I_G/I_D = 1.08$) suggests the more graphitic carbon in the graphene substrate.

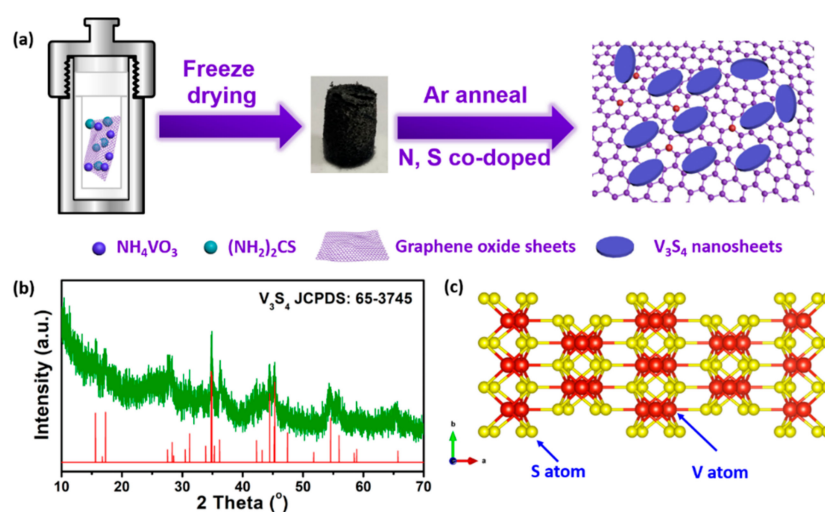


Figure 1. (a) Schematic illustration of preparation process of VS/NSG; (b) XRD pattern of as-prepared VS/NSG; (c) the structure of V_3S_4 along the c -axis.

SEM and TEM were used to characterize the detail morphology and structure of VS/NSG. In the panoramic SEM image (Figure 2a), VS/NSG exhibits morphology typical of nanosheet and graphene composites. Numerous V_3S_4 nanosheets anchor onto the graphene substrate to ensure their electronic conductivity. As shown in the magnified SEM image (Figure 2b), the grown nanosheets display a smooth surface with particles of about $500\text{--}1500\text{ nm}$ in diameter and only $70\text{--}80\text{ nm}$ in width. The composite structure of VS/NSG can be further observed in Figure 2c. The HRTEM (high-resolution transmission electron microscopy) image (Figure 2d) selected from the blue box in Figure 2c displays the clear lattice fringes. Assisted by the fast Fourier transform patterns (FFT, inset of Figure 2d) calculated from the white box region, the interplanar distance can be measured of about 0.567 nm and assigned to the (002) facet of V_3S_4 .

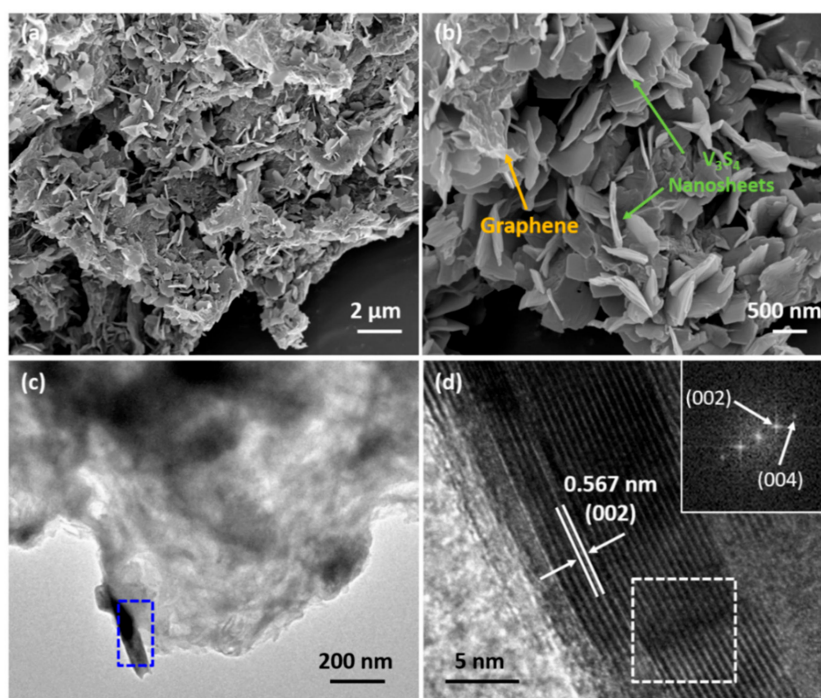


Figure 2. (a,b) SEM images of as-prepared VS/NSG at different magnifications; (c,d) TEM image, HRTEM image, and FFT patterns in the marked white box of VS/NSG.

XPS measurements were carried out to ascertain the surface chemical characteristics of VS/NSG. As shown in Figure S3, the survey spectrum exhibits the peaks of V, S, C, N, and O elements. The high-resolution of V 2p spectrum (Figure 3a) displays four components, corresponding to the V^{2+} and V^{3+} , respectively [7,23]. In Figure 3b, S 2p spectrum exhibits obvious three peaks, which can be assigned to the typical M-S (M = metal), C-S, and common S-O bonds [8,9,24,25]. However, the S 2p spectrum of VS/NSG suggested that the S-doped graphene had been affected by the presence of sulfides. To address this confusion, the graphene substrate formed by the acid-treated VS/NSG was also characterized. As shown in Figure S4, the high-resolution S 2p spectrum of acid-washed sample also displays obvious C-S bonds, confirming that the sulfur had been doped into the graphene. Impressively, the existence of the C-S bond suggests the presence of sulfur covalently bonded to graphene in a heterocyclic configuration [26]. As shown in Figure 3c, four peaks represent the graphitic N, pyrrolic N, pyridinic N, and V-N bond, respectively [27–29]. This result is good verification of the expectation when alien atoms are doped into graphene. Moreover, the obvious V-N bond peak located at 397 eV demonstrates the formation of VN on the surface of VS/NSG, which would enhance the conductivity of as-prepared sample. Moreover, the nitrogen content is about 8.86 at %. The high content of doped nitrogen would be beneficial regarding the improvement of conductivity. The presence of C-N and C-S peaks in the C 1s high-resolution spectrum further confirm the conclusion that N, S co-doped graphene was formed (Figure 3d) [29].

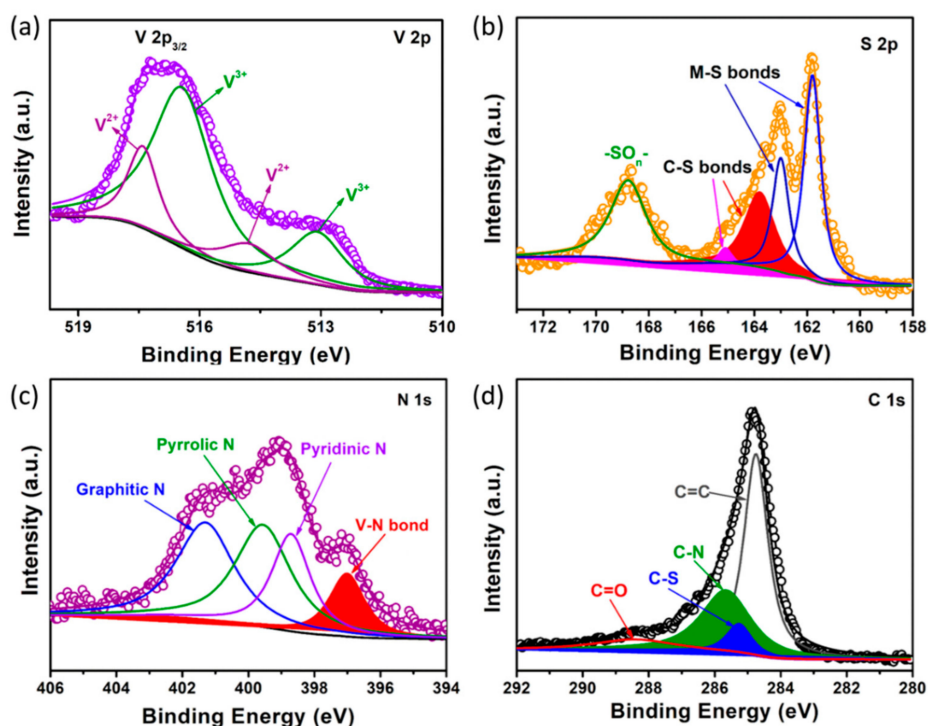


Figure 3. XPS survey (a) V 2p, (b) S 2p, (c) N 1s, and (d) C 1s of as-prepared VS/NSG.

The lithium storage performances of VS/NSG were evaluated by CR2032 half-coin cells. As shown in Figure 4a, in the voltage range of 0.005–3 V under 50 mA g^{-1} , VS/NSG electrode delivers the initial discharge and charge capacity of 1150 and 825 mAh g^{-1} , respectively. The initial coulombic efficiency (ICE) of V_3S_4 nanosheet is about 71.7%, which is much higher than that of other transition metal oxides and sulfides, such as SnO_2 [30], CoO [31], Co_3O_4 [32], V_2O_3 [4], and VS_4 [13]. After the initial cycle, the overlapped discharge–charge curves suggest the well reversibility of as-prepared VS/NSG. Cyclic voltammetry (CV) were used to investigate the lithium storage behavior of V_3S_4 nanosheet. The cathodic peaks located at 1.29, 0.64, and 0.22 V in the first sweep can be assigned to the behavior of Li^+ insertion into V_3S_4 interlayer stepwise and formation of solid electrolyte interface (SEI) layer, respectively [12,13,33]. At the following anodic sweep, the anodic peaks at 1.25, 1.72, and 2.33 V correspond to the delithiation process of $\text{Li}_x\text{V}_3\text{S}_4$ and formation of V_3S_4 [7,17]. The overlapped CV curves at the second and third cycle indicate the good reversibility and cyclic stability of VS/NSG electrode. As shown in Figure 4c, the cyclic stability of VS/NSG were tested under a current density of 2000 mA g^{-1} . At this high current density, VS/NSG electrode delivers an excellent cycling stability. After 400 monotonous cycles, as high as 692 mAh g^{-1} discharge capacity can be retained. The level of coulombic efficiency, being close to 100%, suggests the high reversibility of VS/NSG during the monotonous cycles. As shown in Figure S5, the counterpart of VS/NSG, which without the N, S co-doped graphene substrate delivers the discharge capacity of 856 mAh g^{-1} with the ICE only about 60.1%. In the following cyclic test, the bare cell exhibits obvious capacity fading. In the following rate tests, VS/NSG electrode delivers a high reversible discharge capacity from 0.05 to 10 and back to 0.05 A g^{-1} , which reach 480 and 330 mAh g^{-1} at 5 and 10 A g^{-1} , respectively. Particularly, in the subsequent repetition of rate evaluations, the discharge capacity of VS/NSG at low current densities exhibits an obvious increasing tendency. This phenomenon would be attributed to the increased Li^+ storage ability at the enhanced area of electrolyte and electrode interface. When the current density is back to 0.05 A g^{-1} , a high discharge capacity of 1150 mAh g^{-1} can be retained, indicating the superior rate capability of VS/NSG electrode.

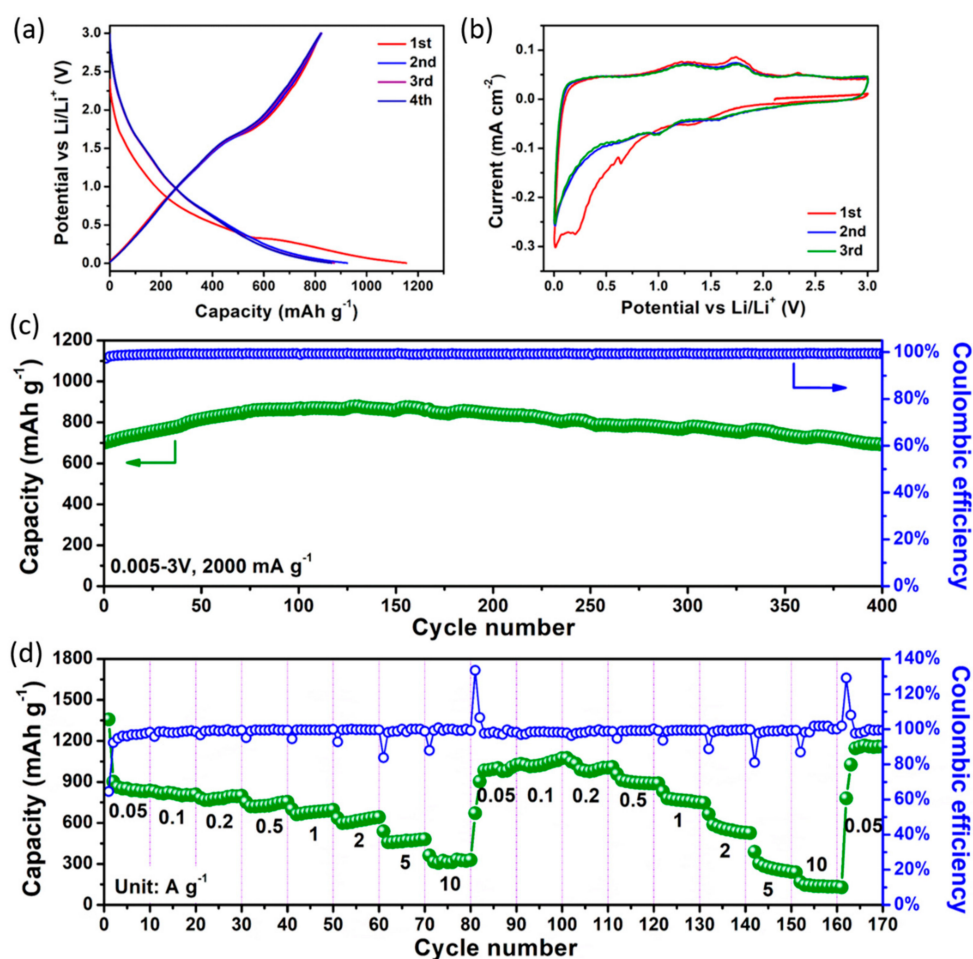


Figure 4. (a) The initial discharge–charge curves of VS/NSG at 0.05 A g⁻¹; (b) CV curves of VS/NSG at a scan rate of 0.1 mV s⁻¹; and (c) the cyclic stability and (d) rate capability of VS/NSG electrode.

Kinetic analyses based on the CV curves were carried out to reveal the potential reasons for the excellent cyclic stability of VS/NSG electrode. At different scanning rates ranging from 0.2 to 1.0 mV s⁻¹ (Figure 5a), the CV curves displayed a similar and broadened shape. The overall charge storage, which is revealed by the integral area of CV curve, could be attributed to by the surface-induced capacitive and diffusion–insertion process [19,34]. Based on the CV curves at different scanning rates and Equation (1) [35], the charge storage mechanism of electrode materials could be studied.

$$i(V) = av^b \quad (1)$$

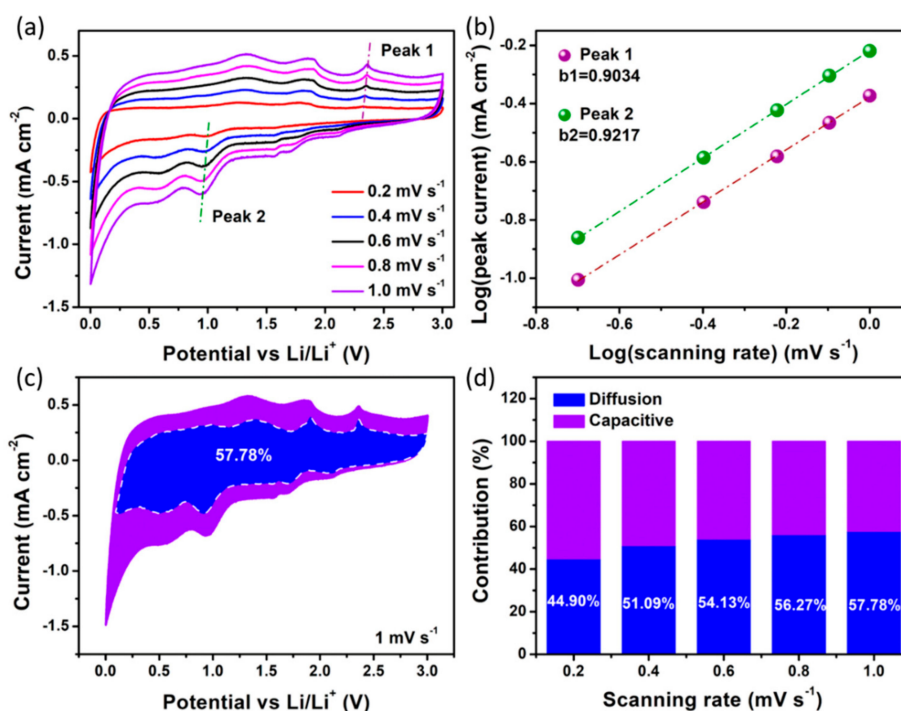


Figure 5. Kinetic analyses of VS/NSG electrode. (a) CV curves at different scanning rates; (b) $\log(i)$ vs. $\log(v)$ plots at different peaks; (c) capacitive contribution (blue region) to the charge storage at 1 mV s^{-1} ; (d) the contribution ratio of pseudocapacitive and diffusion-controlled current at different scanning rates.

According to the previous reports, the value of b in this equation is an indicator to investigate the mechanism of charge storage [20,35]. As shown in Figure 5b, the value of b based on peak 1 and peak 2 is 0.9034 and 0.9217, respectively, which are fitted by the slopes of $\log v$ and $\log i$ (v means the scanning rate and i represents the peak current). These values mean that surface-induced capacitive would be a dominator in VS/NSG electrode charge storage system. The ratio of surface-induced capacitive in the whole charge storage can be further calculated using Equation (2).

$$i(V) = k_1 v + k_2 v^{0.5} \quad (2)$$

The integral area of $k_1 v$ and $k_2 v^{0.5}$ means the surface-induced capacitive and diffusion–insertion process, respectively [36,37]. Furthermore, the values of k_1 at different potentials are the slope of the function of $i(V)/v^{0.5} \sim v^{0.5}$ in a series of CV analyses. Based on the various k_1 at different potential, the profile of surface-induced capacitive under a certain scanning rate could be depicted. As shown in Figure 5c, the blue area represents the charge storage contribution of surface-induced capacitive. The integral area ratio of blue and violet area is 57.78%, meaning the pseudocapacitive contribution is 57.78% at the scanning rate of 1.0 mV s^{-1} . In addition, the surface-induced capacitive profiles and pseudocapacitive contributions from 0.2 to 0.8 mV s^{-1} are depicted in Figure S6 and Figure 5d. The pseudocapacitive contribution is enhanced gradually with the increasing scanning rate, and the ratio at 0.2, 0.4, 0.6, and 0.8 mV s^{-1} is 44.90%, 51.09%, 54.13%, and 56.27%, respectively. Dominant pseudocapacitive effect at fast scanning rate endow the VS/NSG electrode with excellent cyclic stability and rate capability. Moreover, Nyquist plots of VS/NSG electrode at the 3rd and 50th cycle are displayed in Figure S7. Clearly, the smaller semicircle of VS/NSG after 50 cycles, meaning a smaller resistance of charge transfer (R_{st} , an indicator to the degree of side reaction [38–40]), reveals better conductivity due to the increased compatibility of electrode material with electrolyte [41]. The above kinetic analyses indicate that the V_3S_4 nanosheets anchored on N, S co-doped graphene would induce the dominating pseudocapacitive effect and restrain the increasing of R_{st} .

4. Conclusions

In summary, the fabrication of V_3S_4 nanosheets anchored on N, S co-doped graphene by this universal and green method exhibits excellent rate capability and cyclic stability. At the current density of 5 and 10 $A g^{-1}$, the as-prepared VS/NSG delivers a high discharge capacity of 480 and 330 $mAh g^{-1}$, respectively. At the end of 400 cycles under 2 $A g^{-1}$, 692 $mAh g^{-1}$ also can be retained. The superior electrochemical performances of VS/NSG benefited by the formed N, S co-doped graphene aerogel, not only endow it with an enhanced capability to buffer the volume expansion, but also a constructed conductive network that improves its electron conductivity. Moreover, the dominant pseudocapacitive contribution at fast scanning rate and the decreasing resistance of charge transfer also guarantee fast and durable Li^+ storage performance.

Supplementary Materials: The following are available online at <http://www.mdpi.com/2079-4991/9/11/1638/s1>, Figure S1: TG curve of V_3S_4/N , S-rGO nanosheets under air atmosphere, Figure S2: Raman spectrum of VS/NSG sample, Figure S3: XPS spectrum of as-prepared V_3S_4/N , S-rGO nanosheets, Figure S4: XPS S 2p spectrum of VS/NSG treated after acid, Figure S5: (a) Initial discharge-charge curves and (b) cyclic performance of V_3S_4 counterpart under 0.05 and 0.5 $A g^{-1}$, respectively. Figure S6: Capacitive current contribution (blue region) to the charge storage at (a) 0.2, (b) 0.4, (c) 0.6 and (d) 0.8 $mV s^{-1}$ of V_3S_4/N , S-rGO nanosheets, Figure S7: Nyquist plots of V_3S_4/N , S-rGO nanosheets cell at 3rd and after 50 cycles.

Author Contributions: Conceptualization and methodology, N.W. and X.L.; data and experiment curation, D.M., X.Z. and N.W.; formal analysis, L.Z., G.L., D.G. and N.W.; writing—original draft preparation, N.W.; writing—review and editing, N.W. and X.L.; funding acquisition, N.W.

Funding: This work was financially supported by National Natural Science Foundation of China (No. 51804156), the Program for Science & Technology Innovation Talents in Universities of Henan Province (No. 20HASTIT020), the Colleges and Universities in Henan Province Key Science and Research Project (No. 18A430002), Henan Province Science and Technology Tackle Key Problems Project (No.182102310908).

Conflicts of Interest: The authors declare no conflict of interest.

References

1. Liu, J.; Wang, J.; Xu, C.; Jiang, H.; Li, C.; Zhang, L.; Lin, J.; Shen, Z.X. Advanced Energy Storage Devices: Basic Principles, Analytical Methods, and Rational Materials Design. *Adv. Sci.* **2018**, *5*, 1700322. [[CrossRef](#)] [[PubMed](#)]
2. Ni, S.; Liu, J.; Chao, D.; Mai, L. Vanadate-Based Materials for Li-Ion Batteries: The Search for Anodes for Practical Applications. *Adv. Energy Mater.* **2019**, *9*, 1803324. [[CrossRef](#)]
3. Jiang, L.; Qu, Y.; Ren, Z.; Yu, P.; Zhao, D.; Zhou, W.; Wang, L.; Fu, H. In Situ Carbon-Coated Yolk-Shell V_2O_3 Microspheres for Lithium-Ion Batteries. *ACS Appl. Mater. Interfaces* **2015**, *7*, 1595–1601. [[CrossRef](#)] [[PubMed](#)]
4. Zeng, L.; Zheng, C.; Xi, J.; Fei, H.; Wei, M. Composites of V_2O_3 -ordered mesoporous carbon as anode materials for lithium-ion batteries. *Carbon* **2013**, *62*, 382–388. [[CrossRef](#)]
5. Pan, J.; Zhong, L.; Li, M.; Luo, Y.; Li, G. Microwave-Assisted Solvothermal Synthesis of VO_2 Hollow Spheres and Their Conversion into V_2O_5 Hollow Spheres with Improved Lithium Storage Capability. *Chem. Eur. J.* **2016**, *22*, 1461–1466. [[CrossRef](#)] [[PubMed](#)]
6. Ding, Y.; Wen, Y.; Wu, C.; van Aken, P.A.; Maier, J.; Yu, Y. 3D V_6O_{13} Nanotextiles Assembled from Interconnected Nanogrooves as Cathode Materials for High-Energy Lithium Ion Batteries. *Nano Lett.* **2015**, *15*, 1388–1394. [[CrossRef](#)]
7. Liu, Q.; Yao, W.; Zhan, L.; Wang, Y.; Zhu, Y. V_3S_4 nanoparticles anchored on three-dimensional porous graphene gel for superior lithium storage. *Electrochim. Acta* **2018**, *261*, 35–41. [[CrossRef](#)]
8. Xiong, X.; Wang, G.; Lin, Y.; Wang, Y.; Ou, X.; Zheng, F.; Yang, C.; Wang, J.; Liu, M. Enhancing Sodium Ion Battery Performance by Strongly Binding Nanostructured Sb_2S_3 on Sulfur-Doped Graphene Sheets. *ACS Nano* **2016**, *10*, 10953–10959. [[CrossRef](#)]
9. Gao, X.; Wang, B.; Zhang, Y.; Liu, H.; Liu, H.; Wu, H.; Dou, S. Graphene-scroll-sheathed α -MnS coaxial nanocables embedded in N, S Co-doped graphene foam as 3D hierarchically ordered electrodes for enhanced lithium storage. *Energy Storage Mater.* **2019**, *16*, 46–55. [[CrossRef](#)]

10. Yu, D.; Pang, Q.; Gao, Y.; Wei, Y.; Wang, C.; Chen, G.; Du, F. Hierarchical Flower-like VS₂ Nanosheets-A High Rate-Capacity and Stable Anode Material for Sodium-ion Battery. *Energy Storage Mater.* **2018**, *11*, 1–7. [[CrossRef](#)]
11. Zhou, Y.; Li, Y.; Yang, J.; Tian, J.; Xu, H.; Yang, J.; Fan, W. Conductive Polymer-Coated VS₄ Submicrospheres as Advanced Electrode Materials in Lithium-Ion Batteries. *ACS Appl. Mater. Interfaces* **2016**, *8*, 18797–18805. [[CrossRef](#)] [[PubMed](#)]
12. Zhou, Y.; Tian, J.; Xu, H.; Yang, J.; Qian, Y. VS₄ Nanoparticles Rooted by a-C Coated MWCNTs as an Advanced Anode Material in Lithium Ion Batteries. *Energy Storage Mater.* **2017**, *6*, 149–156. [[CrossRef](#)]
13. Yang, G.; Wang, H.; Zhang, B.; Foo, S.; Ma, M.; Cao, X.; Liu, J.; Ni, S.; Srinivasan, M.; Huang, Y. Superior Li-ion storage of VS₄ nanowires anchored on reduced graphene. *Nanoscale* **2019**, *11*, 9556–9562. [[CrossRef](#)] [[PubMed](#)]
14. Zhu, L.; Li, Y.; Wang, J.; Zhu, X. Sodium storage performance and mechanism of rGO-wrapped nanorod vanadium sulfide as an anode material for sodium ion batteries. *Solid State Ionics* **2018**, *327*, 129–135. [[CrossRef](#)]
15. Shen, L.; Wang, Y.; Wu, F.; Moudrakovski, I.; Aken, P.A.; Maier, J.; Yu, Y. Hierarchical Metal Sulfide/Carbon Spheres: A Generalized Synthesis and High Sodium-Storage Performance. *Angew. Chem. Int. Ed.* **2019**, *58*, 7238–7243. [[CrossRef](#)] [[PubMed](#)]
16. Yang, C.; Ou, X.; Xiong, X.; Zheng, F.; Hu, R.; Chen, Y.; Liu, M.; Huang, K. V₅S₈-graphite hybrid nanosheets as a high rate-capacity and stable anode material for sodium-ion batteries. *Energy Environ. Sci.* **2017**, *10*, 107–113. [[CrossRef](#)]
17. Ou, X.; Liang, X.; Zheng, F.; Pan, Q.; Zhou, J.; Xiong, X.; Yang, C.; Hu, R.; Liu, M. Exfoliated V₅S₈/graphite nanosheet with excellent electrochemical performance for enhanced lithium storage. *Chem. Eng. J.* **2017**, *320*, 485–493. [[CrossRef](#)]
18. Rout, C.S.; Kim, B.; Xu, X.; Yang, J.; Jeong, H.Y.; Odkhuu, D.; Park, N.; Cho, J.; Shin, H.S. Synthesis and characterization of patronite form of vanadium sulfide on graphitic layer. *J. Am. Chem. Soc.* **2013**, *135*, 8720–8725. [[CrossRef](#)]
19. Wu, N.; Tian, W.; Shen, J.; Qiao, X.; Sun, T.; Wu, H.; Zhao, J.; Liu, X.; Zhang, Y. Facile fabrication of a jarosite ultrathin KFe₃(SO₄)₂(OH)₆@rGO nanosheet hybrid composite with pseudocapacitive contribution as a robust anode for lithium-ion batteries. *Inorg. Chem. Front.* **2019**, *6*, 192–198. [[CrossRef](#)]
20. Wu, N.; Shen, J.; Sun, L.; Yuan, M.; Shao, Y.; Ma, J.; Liu, G.; Guo, D.; Liu, X.; He, Y. Hierarchical N-doped graphene coated 1D cobalt oxide microrods for robust and fast lithium storage at elevated temperature. *Electrochim. Acta* **2019**, *310*, 70–77. [[CrossRef](#)]
21. Cho, J.S.; Park, S.; Jeon, K.M.; Piao, Y.; Kang, Y.C. Mesoporous reduced graphene oxide/WSe₂ composite particles for efficient sodium-ion batteries and hydrogen evolution reactions. *Appl. Surf. Sci.* **2018**, *459*, 309–317. [[CrossRef](#)]
22. Cho, J.S.; Lee, S.Y.; Lee, J.K.; Kang, Y.C. Iron Telluride-Decorated Reduced Graphene Oxide Hybrid Microspheres as Anode Materials with Improved Na-Ion Storage Properties. *ACS Appl. Mater. Interfaces* **2016**, *8*, 21343–21349. [[CrossRef](#)] [[PubMed](#)]
23. Silversmit, G.; Depla, D.; Poelman, H.; Marin, G.B.; De Gryse, R. Determination of the V 2p XPS binding energies for different vanadium oxidation states (V⁵⁺ to V⁰⁺). *J. Electron Spectrosc.* **2004**, *135*, 167–175. [[CrossRef](#)]
24. Liu, Y.; Liu, X.; Liu, G.; Cui, J.; Luo, R.; Huang, X.; Wu, N.; Jin, X.; Chen, H.; Tang, S.; et al. 2D MoS₂ grown on biomass-based hollow carbon fibers for energy storage. *Appl. Surf. Sci.* **2019**, *469*, 854–863. [[CrossRef](#)]
25. Wang, L.; Hu, L.; Yang, W.; Liang, D.; Liu, L.; Liang, S.; Yang, C.; Fang, Z.; Dong, Q.; Deng, C. N/S-Co-Doped Porous Carbon Sheets Derived from Bagasse as High-Performance Anode Materials for Sodium-Ion Batteries. *Nanomaterials* **2019**, *9*, 1203. [[CrossRef](#)]
26. Liu, T.; Zhang, L.; Tian, Y. Earthworm-like N, S-Doped carbon tube-encapsulated Co₉S₈ nanocomposites derived from nanoscaled metal-organic frameworks for highly efficient bifunctional oxygen catalysis. *J. Mater. Chem. A* **2018**, *6*, 5935–5943. [[CrossRef](#)]
27. Lee, W.J.; Lim, J.; Kim, S.O. Nitrogen Dopants in Carbon Nanomaterials: Defects or a New Opportunity? *Small Methods* **2017**, *1*, 1600014. [[CrossRef](#)]
28. Wang, J.; Yang, C.; Wu, J.; Zhang, L.; Wei, M. Facile synthesis of VN hollow spheres as an anode for lithium-ion battery. *J. Electroanal. Chem.* **2019**, *848*, 113360. [[CrossRef](#)]

29. Balamurugan, J.; Karthikeyan, G.; Thanh, T.D.; Kim, N.H.; Lee, J.H. Facile synthesis of vanadium nitride/nitrogen-doped graphene composite as stable high performance anode materials for supercapacitors. *J. Power Sour.* **2016**, *308*, 149–157. [[CrossRef](#)]
30. Li, Z.; Yin, Q.; Hu, W.; Zhang, J.; Guo, J.; Chen, J.; Sun, T.; Du, C.; Shu, J.; Yu, L.; et al. Tin/tin antimonide alloy nanoparticles embedded in electrospun porous carbon fibers as anode materials for lithium-ion batteries. *J. Mater. Sci.* **2019**, *54*, 9025–9033. [[CrossRef](#)]
31. Wu, F.; Zhang, S.; Xi, B.; Feng, Z.; Sun, D.; Ma, X.; Zhang, J.; Feng, J.; Xiong, S. Unusual Formation of CoO@C “Dandelions” Derived from 2D Kagomé MOFs for Efficient Lithium Storage. *Adv. Energy Mater.* **2018**, *8*, 1703242. [[CrossRef](#)]
32. Zeng, H.; Xing, B.; Chen, L.; Yi, G.; Huang, G.; Yuan, R.; Zhang, C.; Cao, Y.; Chen, Z. Nitrogen-Doped Porous Co₃O₄/Graphene Nanocomposite for Advanced Lithium-Ion Batteries. *Nanomaterial* **2019**, *9*, 1253. [[CrossRef](#)] [[PubMed](#)]
33. Britto, S.; Leskes, M.; Hua, X.; Hebert, C.A.; Shin, H.S.; Clarke, S.; Borkiewicz, O.; Chapman, K.W.; Seshadri, R.; Cho, J.; et al. Multiple Redox Modes in the Reversible Lithiation of High-Capacity, Peierls-Distorted Vanadium Sulfide. *J. Am. Chem. Soc.* **2015**, *137*, 8499–8508. [[CrossRef](#)] [[PubMed](#)]
34. Kim, H.; Cook, J.B.; Lin, H.; Ko, J.S.; Tolbert, S.H.; Ozolins, V.; Dunn, B. Oxygen vacancies enhance pseudocapacitive charge storage properties of MoO_{3-x}. *Nat. Mater.* **2016**, *16*, 454–460. [[CrossRef](#)] [[PubMed](#)]
35. Augustyn, V.; Come, J.; Lowe, M.A.; Kim, J.W.; Taberna, P.; Tolbert, S.H.; Abruna, A.H.D.; Simon, P.; Dunn, B. High-rate electrochemical energy storage through Li⁺ intercalation pseudocapacitance. *Nat. Mater.* **2013**, *12*, 518–522. [[CrossRef](#)] [[PubMed](#)]
36. Deng, X.; Wei, Z.; Cui, C.; Liu, Q.; Wang, C.; Ma, J. Oxygen-deficient anatase TiO₂@C nanospindles with pseudocapacitive contribution for enhancing lithium storage. *J. Mater. Chem. A* **2018**, *6*, 4013–4022. [[CrossRef](#)]
37. Wu, N.; Wu, H.; Qiao, X.; Shen, J.; Liu, X.; Liu, G.; Sun, T.; Hou, H.; Zhang, Y.; Ji, X. Anatase inverse opal TiO_{2-x}@N-doped C induced the dominant pseudocapacitive effect for durable and fast lithium/sodium storage. *Electrochim. Acta* **2019**, *299*, 540–548. [[CrossRef](#)]
38. Cho, J.S.; Lee, J.K.; Kang, Y.C. Graphitic Carbon-Coated FeSe₂ Hollow Nanosphere-Decorated Reduced Graphene Oxide Hybrid Nanofibers as an Efficient Anode Material for Sodium Ion Batteries. *Sci. Rep.* **2016**, *6*, 23699. [[CrossRef](#)]
39. Cho, J.S.; Lee, S.Y.; Kang, Y.C. First Introduction of NiSe₂ to Anode Material for Sodium-Ion Batteries: A Hybrid of Graphene-Wrapped NiSe₂/C Porous Nanofiber. *Sci. Rep.* **2016**, *6*, 23338. [[CrossRef](#)]
40. Wu, N.; Wu, H.; Kim, J.; Liu, X.; Zhang, Y. Restoration of Degraded Nickel-Rich Cathode Materials for Long-Life Lithium-Ion Batteries. *Chemelectrochem* **2018**, *5*, 78–83. [[CrossRef](#)]
41. Wang, F.; Liu, Y.; Zhao, Y.; Wang, Y.; Wang, Z.; Zhang, W.; Ren, F. Facile Synthesis of Two-Dimensional Porous MgCo₂O₄ Nanosheets as Anode for Lithium-Ion Batteries. *Appl. Sci.* **2018**, *8*, 22. [[CrossRef](#)]

